Supporting Information

Probing key organic substances driving new particle growth initiated by iodine nucleation in coastal atmosphere

Yibei Wan,[1] Xiangpeng Huang,[2] Bin Jiang,[3] Binyu Kuang,[4] Manfei Lin,[4] Deming Xia[5], Yuhong Liao,[3] Jingwen Chen,[5] Jianzhen Yu,[4] and Huan Yu[1]

[1] Department of Atmospheric Science, School of Environmental Studies, China University of Geosciences, Wuhan, 430074, China

[2] School of Environmental Science and Engineering, Nanjing University of Information Science and Technology, Nanjing, 210044, China

[3] Guangzhou Institute of Geochemistry, Chinese Academy of Sciences, Guangzhou 510640, China

[4] Department of Chemistry, Hong Kong University of Science & Technology, Clear Water Bay, Kowloon, Hong Kong, China

[5] School of Environmental Science and Technology, Dalian University of Technology, Dalian 116024, China

Corresponding author: H. Yu (yuhuan@cug.edu.cn)

Text:

ESI-FT-ICR MS operation conditions

Figures:

Figure S1: Particle number size distribution spectra monitored by a SMPS and a NAIS at Xiangshan gulf of China during the 3 nano-MOUDI sampling periods. (a) Iodine initiated NPF days from 9 to 11 May, (b) continental regional NPF days from 11 to 13 February, (c) the non-NPF days from 16 to 18 April.

Figure S2. Reconstructed mass spectra of the 7 elemental groups in ESI-and ESI+ modes for the four size bins.

Figure S3: DBE vs. C atom number diagrams of all the CHON and CHO formulas detected in 10–18 nm particles in ESI+ mode. (a) (b) +H adducts, (c) (d) +Na adducts. The color bar denotes the O number in the formulas. The size of the circles reflects the relative intensities of molecular formulas on a logarithmic scale.

Figure S4: Relative intensities of subgroups according to O atom number in CHON, CHO, CHONI and CHOI formulas in the four size bins in ESI+ (in red) and ESI- (in blue). The intensity of the most abundant subgroup is defined as 1 and those of other subgroups are normalized by it. The relative intensities of non-iodinated OC formulas (iodinated OC formulas) are plotted in the region above (below) zero line.

Figure S5: O atom number of *vs.* N atom number of $C_{10}H_xO_yN_z$ compounds detected in 180–560 nm particles (a) and $C_{18}H_xO_yN_z$ compounds detected in 10–18 nm particles in ESI- mode (b).

Figure S6: Simplified reaction scheme showing the formation of oxygenated and nitrated CHO and CHON compounds from α-linolenic acid oxidation in the atmosphere.

Figure S7: Simplified reaction scheme showing the formation of oxygenated CHO compounds from unsaturated C_{28} FA ($C_{28}H_{52}O_2$) oxidation in the atmosphere.

Figure S8: Simplified reaction scheme showing the formation of oxygenated CHON compounds containing a $–NH_2$ group from unsaturated C_{18} amino alcohol ($C_{18}H_{37}NO_4$) oxidation in the atmosphere.

Tables:

Table S1. Predicted saturation concentration (C*) range of most abundant CHON and CHO formulas, as well as their possible precursors.

ESI-FT-ICR MS operation conditions

A syringe pump infused the sample extract continuously into the ESI unit with a flow rate of 180 μL h-1. The ESI source conditions were as follows: the nebulizer gas pressure was 1 bar; the dry gas (N_2) pressure was 4 bar and its temperature was 200 °C; the capillary voltage was 4.5 kV. The ion accumulation time in the argon-filled hexapole collision pool with 1.5 V of direct current voltage and 1400 Vp-p of radio frequency (RF) amplitude was 0.05 s, followed by transport ions through a hexapole ion guide to the ICR cell for 0.7 ms. 4 M words of data were recorded over the mass range of 150-1000 Da for each run. A total of 128 scans were collected to enhance the signal/noise (S/N) ratio and dynamic range.

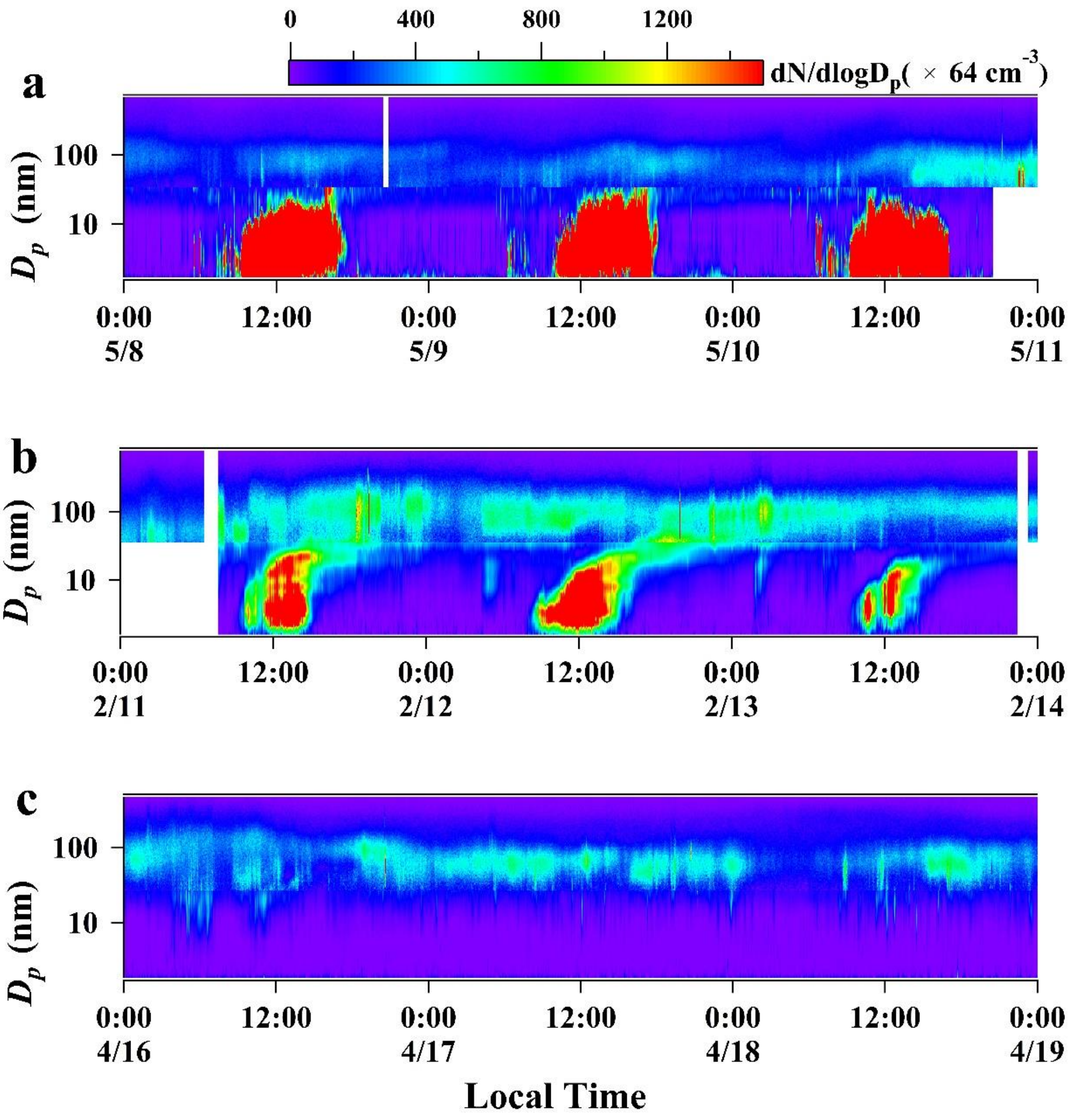

Figure S1. Particle number size distribution spectra monitored by a SMPS and a NAIS during the 3 nano-MOUDI sampling periods. (a) Iodine-initiated NPF (I-NPF) days from May 9 to 11, (b) continental regional NPF (C-NPF) days from February 11 to 13, (c) non-NPF days from April 16 to 18.

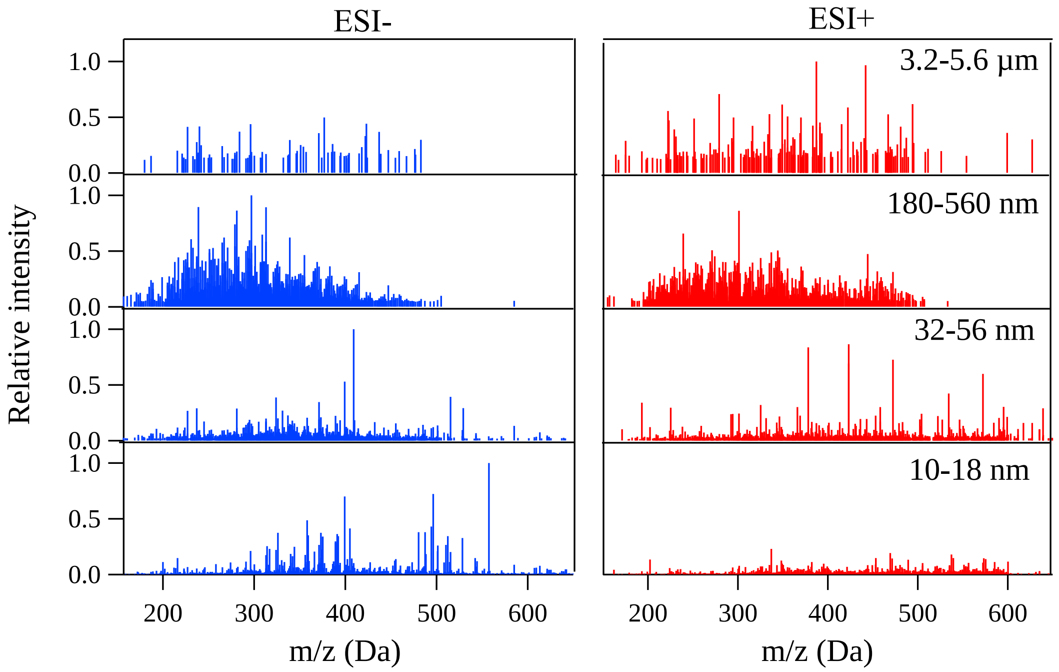

Figure S2. Reconstructed mass spectra of the 7 elemental groups in ESI- (left panels) and ESI+ (right panels) modes for the four size bins. The signals are normalized against the intensity of the most abundant molecular ions in a size bin.

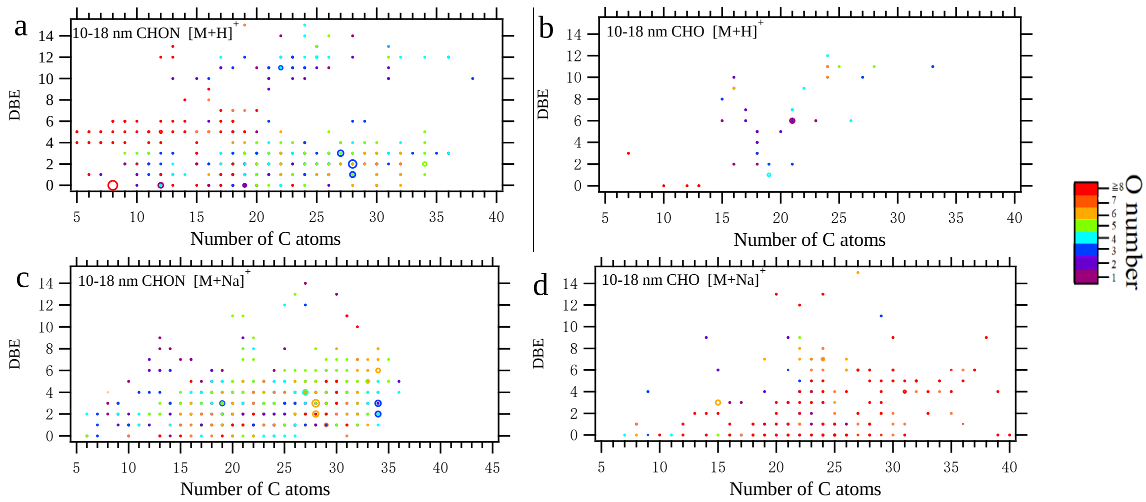

Figure S3. DBE vs. C atom number diagrams of all CHON and CHO formulas detected in 10–18 nm particles in ESI+ mode. (a) (b) $[M+H]^+$ adducts, (c) (d) $[M+Na]^+$ adducts. The color bar denotes O number in the formulas. The size of the circles reflects the relative intensities of molecular formulas on a logarithmic scale.

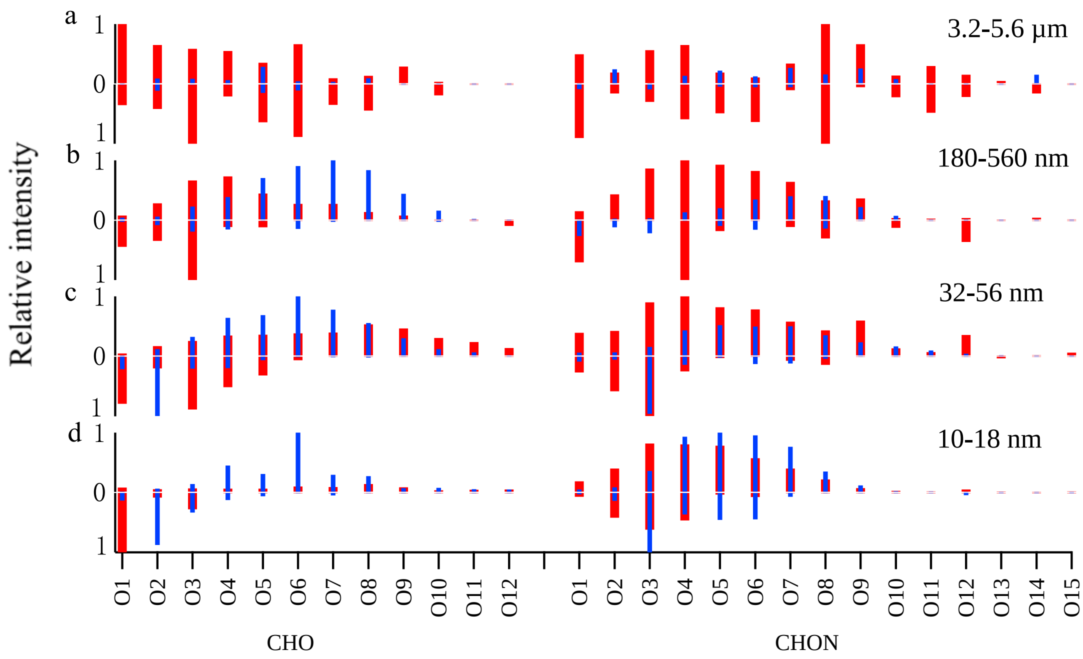

Figure S4. Relative intensities of subgroups according to O atom number in CHON, CHO, CHONI and CHOI formulas in the four size bins in ESI+ (in red) and ESI- (in blue). The intensity of the most abundant subgroup in a size bin is defined as 1 and those of other subgroups are normalized by it. The relative intensities of non-iodinated OC formulas (iodinated OC formulas) are plotted in the region above (below) zero line.

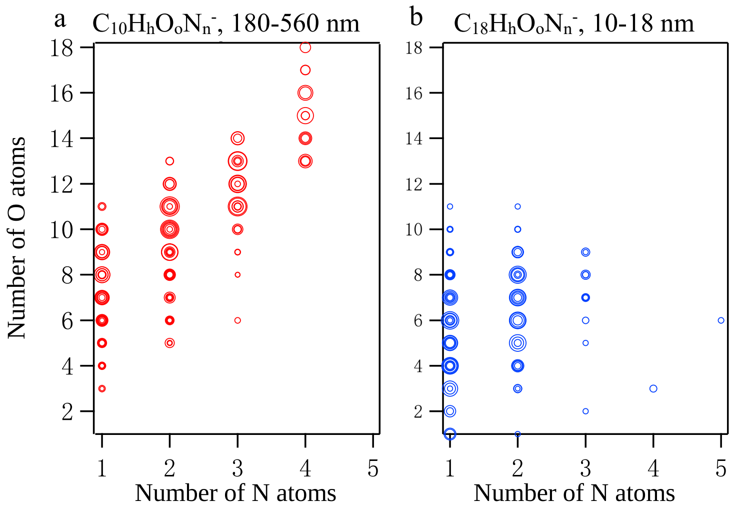

Figure S5. O atom number of *vs.* N atom number of $C_{10}H_hO_oN_n^-$ compounds detected in 180–560 nm particles (a) and $C_{18}H_hO_oN_n$- compounds detected in 10–18 nm particles in ESI- mode (b).

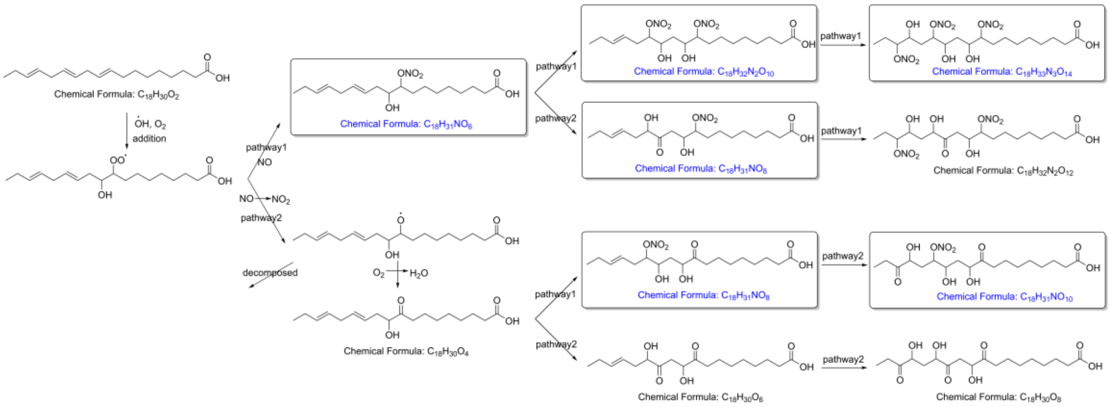

Figure S6. Simplified reaction scheme of the formation of oxygenated and nitrated CHO and CHON compounds from α-linolenic acid ($C_{18}H_{30}O_2$) oxidation in the atmosphere. One representative structure is shown for each chemical formula. Chemical formulas in the boxes are found in the formula list detected in 10–18 nm particles. Pathway 1: OH and O_2 addition followed by reaction with NO to form a –ONO_2 group; pathway 2: OH and O_2 addition followed by reaction with NO to form an alkoxy radical that further reacts with O_2 to form a –C=O group.

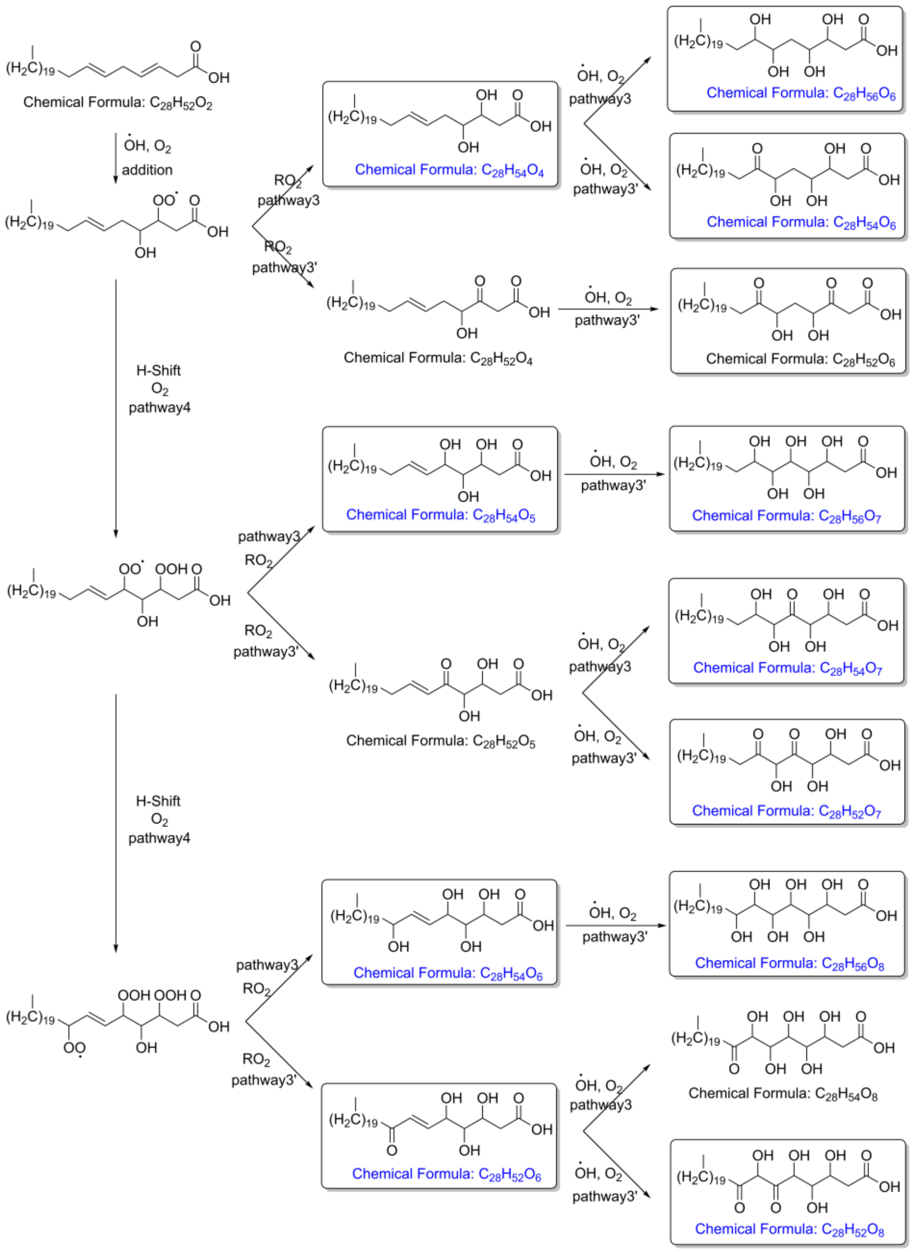

Figure S7. Simplified reaction scheme of the formation of oxygenated CHO compounds from unsaturated C_{28} FA ($C_{28}H_{52}O_2$) oxidation in the atmosphere. One representative structure is shown for each chemical formula. Chemical formulas in the boxes are found in the formula list detected in 10–18 nm particles. Pathway 3: OH and O_2 addition followed by reaction with RO_2 to form a –OH or a –C=O group; Pathway 4: successive intermolecular H-shift/O_2 addition (autoxidation) to form RO_2 radicals with –OOH group. –OOH group is not stable and decomposed to -OH.

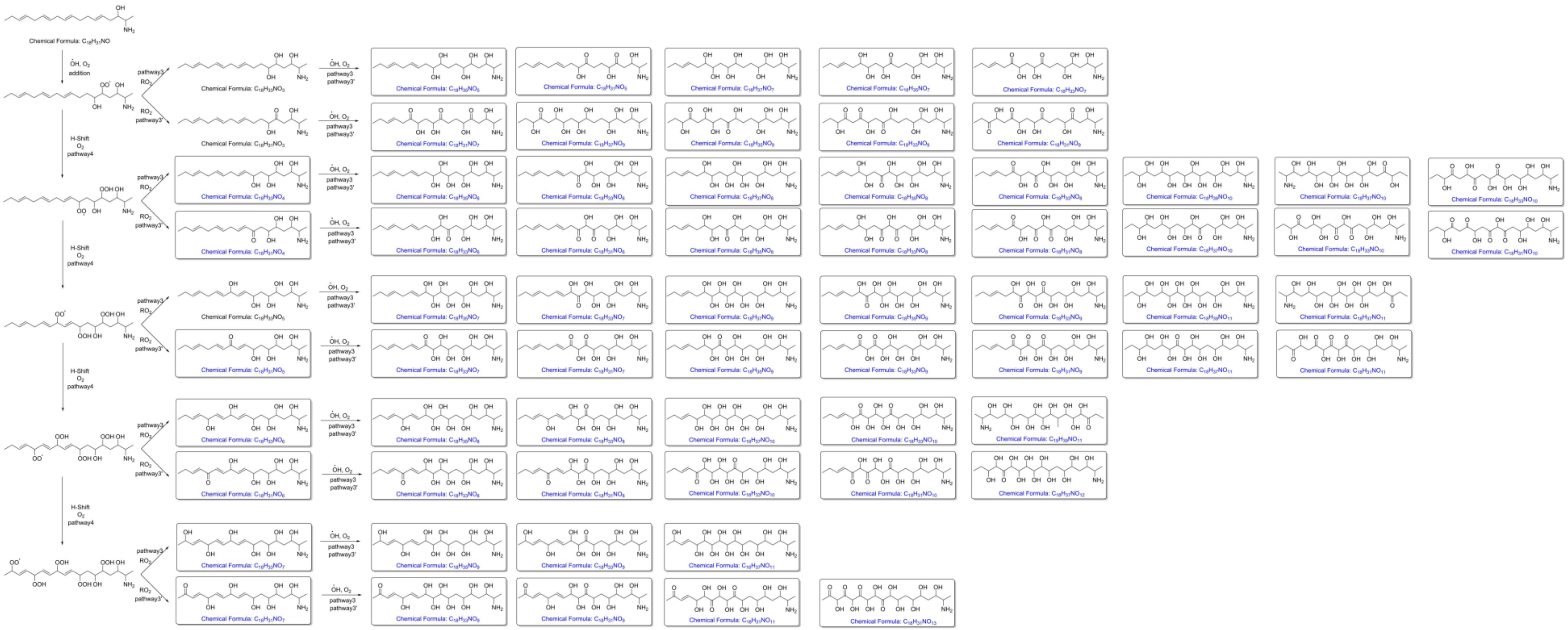

Figure S8. Simplified reaction scheme of the formation of oxygenated CHON compounds containing a –NH_2 group from unsaturated C_{18} amino alcohol ($C_{18}H_{37}NO_4$) oxidation in the atmosphere. One representative structure is shown for each chemical formula. Chemical formulas in the boxes are found in the formula list detected in 10–18 nm particles. Pathway 3: OH and O_2 addition followed by reaction with RO_2 to form a –OH or a –C=O group; Pathway 4: successive intermolecular H-shift/O_2 addition autoxidation to form RO_2 radicals with –OOH group.

Table S1. Predicted saturation concentration (C*) range of most abundant CHON and CHO formulas, as well as their possible precursors.

Formula	Predicted C^* (μg m^{-3})	Predicted C^* of possible precursors (μg m^{-3})
	ESI- mode	
$C_{18}H_{33}NO_4$	1.62×10^{-5}–2.06×10^{-2}	3.40×10^{-1}–8.91
$C_{18}H_{33}NO_6$	7.66×10^{-10}–1.33×10^{-2}	3.40×10^{-1}–88.7
$C_{18}H_{34}N_2O_6$	7.62×10^{-11}–1.32×10^{-3}	3.40×10^{-2}–8.91
$C_{18}H_{34}N_2O_7$	5.21×10^{-13}–9.06×10^{-6}	3.40×10^{-2}–8.91
$C_{18}H_{34}N_2O_8$	1.30×10^{-15}–5.56×10^{-6}	3.40×10^{-2}–8.91
$C_{18}H_{36}N_2O_5$	1.44×10^{-8}–1.10×10^{-2}	3.40×10^{-2}–88.7
$C_{18}H_{36}N_2O_6$	9.83×10^{-11}–7.54×10^{-5}	3.40×10^{-2}–88.7
$C_{18}H_{36}N_2O_7$	6.72×10^{-13}–5.15×10^{-7}	3.40×10^{-2}–88.7
$C_{19}H_{39}NO_7$	3.40×10^{-12}–1.15×10^{-7}	1.34 × 10-01–35.1
$C_{30}H_{57}NO_4$	7.44×10^{-8}–6.69×10^{-6}	4.29×10^{-6}–1.16×10^{-3}
$C_{30}H_{59}NO_3$	5.58×10^{-9}–1.58×10^{-6}	4.29×10^{-6}–1.14×10^{-4}
$C_{30}H_{59}NO_4$	6.28×10^{-10}–8.62×10^{-6}	4.29×10^{-6}–1.16×10^{-3}
$C_{30}H_{59}NO_5$	4.52×10^{-12}–1.32×10^{-6}	4.29×10^{-6}–1.16×10^{-3}
$C_{30}H_{59}NO_6$	2.64×10^{-13}–8.93×10^{-9}	4.29×10^{-6}–1.16×10^{-3}
$C_{30}H_{60}O_6$	1.66×10^{-14}–3.76×10^{-13}	4.36×10^{-5}–1.16×10^{-3}
$C_{20}H_{40}O_6$	2.13×10^{-10}–4.83×10^{-9}	5.28 × 10-01–13.9
$C_{21}H_{42}O_6$	8.32×10^{-11}–1.88×10^{-9}	2.07 × 10-01–5.46
$C_{22}H_{44}O_4$	6.95×10^{-7}–1.57×10^{-5}	8.15×10^{-2}–2.15
$C_{24}H_{48}O_4$	1.06×10^{-7}–2.39×10^{-6}	1.25×10^{-2}–0.330
$C_{26}H_{52}O_4$	1.60×10^{-8}–3.63×10^{-7}	1.90×10^{-3}–5.05×10^{-2}
$C_{27}H_{54}O_6$	2.87×10^{-13}–6.49×10^{-12}	7.42×10^{-4}–1.97×10^{-2}
$C_{28}H_{56}O_4$	2.41×10^{-9}–5.47×10^{-8}	2.89×10^{-4}–7.67×10^{-3}
$C_{28}H_{56}O_6$	1.11×10^{-13}–2.51×10^{-12}	2.89×10^{-4}–7.67×10^{-3}
$C_{29}H_{58}O_6$	4.29×10^{-14}–9.73×10^{-13}	1.12×10^{-4}–2.98×10^{-3}
$C_{33}H_{66}O_6$	9.56×10^{-16}–2.17×10^{-14}	2.54×10^{-6}–6.77×10^{-5}
$C_{38}H_{76}O_8$	3.66×10^{-22}–8.30×10^{-21}	2.18×10^{-8}–5.85×10^{-7}
	ESI+ mode	
$C_{11}H_{18}N_4O_8$	4.73×10^{-9}–3.63×10^{-3}	2.21–$5.61 \times 10^{+2}$
$C_{12}H_{20}N_4O_8$	1.85×10^{-9}–1.42×10^{-3}	0.885–$2.26 \times 10^{+2}$
$C_{19}H_{35}NO_3$	9.26×10^{-4}	1.34×10^{-01}–0.223
$C_{19}H_{36}N_2O_5$	4.35×10^{-9}–3.34×10^{-3}	1.34×10^{-01}–3.52
$C_{19}H_{37}NO_3$	1.20×10^{-3}–2.71×10^{-2}	1.34×10^{-01}–0.223

$C_{19}H_{38}N_2O_3$	2.71×10^{-3}–5.04×10^{-3}	1.34×10^{-2}–3.52
$C_{24}H_{46}N_2O_4$	5.73×10^{-9}–4.39×10^{-3}	1.24×10^{-4}–3.28×10^{-2}
$C_{25}H_{43}NO_4$	3.07×10^{-7}–1.72×10^{-5}	4.83×10^{-4}–1.28×10^{-2}
$C_{26}H_{51}NO_5$	1.73×10^{-9}	1.88×10^{-4}–3.13×10^{-4}
$C_{27}H_{50}N_2O_4$	6.42×10^{-10}–3.29×10^{-7}	7.23×10^{-6}–1.95×10^{-3}
$C_{27}H_{50}N_2O_5$	3.11×10^{-11}–1.05×10^{-6}	7.23×10^{-6}–1.95×10^{-3}
$C_{27}H_{52}N_2O_3$	4.94×10^{-8}–2.76×10^{-6}	7.23×10^{-6}–1.95×10^{-3}
$C_{28}H_{52}N_2O_6$	1.14×10^{-14}–8.03×10^{-8}	2.81×10^{-6}–7.57×10^{-4}
$C_{28}H_{54}N_2O_6$	5.95×10^{-15}–1.03×10^{-7}	2.81×10^{-6}–7.57×10^{-4}
$C_{28}H_{56}N_2O_3$	6.09×10^{-8}–1.38×10^{-6}	2.81×10^{-6}–7.57×10^{-4}
$C_{28}H_{56}N_2O_6$	1.89×10^{-14}–5.88×10^{-9}	2.81×10^{-6}–7.57×10^{-4}
$C_{28}H_{58}N_2O_3$	3.18×10^{-8}	2.81×10^{-6}–4.66×10^{-6}
$C_{29}H_{56}N_2O_6$	2.30×10^{-15}–3.99×10^{-8}	1.09×10^{-6}–2.94×10^{-4}
$C_{29}H_{59}NO_7$	2.85×10^{-17}–6.47×10^{-16}	1.11×10^{-5}–2.94×10^{-4}
$C_{33}H_{59}NO_5$	1.05×10^{-12}–3.02×10^{-8}	2.49×10^{-7}–6.65×10^{-6}
$C_{34}H_{59}NO_6$	2.13×10^{-15}–1.38×10^{-9}	9.64×10^{-8}–2.57×10^{-6}
$C_{34}H_{66}N_2O_3$	1.15×10^{-11}–3.58×10^{-9}	9.45×10^{-9}–2.57×10^{-6}
$C_{34}H_{68}N_2O_3$	2.03×10^{-10}–4.61×10^{-9}	9.45×10^{-9}–2.57×10^{-6}
$C_{34}H_{68}N_2O_5$	3.75×10^{-15}–2.88×10^{-9}	9.45×10^{-9}–2.57×10^{-6}